The 21st-century wetting inhibits growing surface ozone in Northwestern China

Authors: Xiaodong Zhang[1,*], Yu Yan[2], Ning Zhang[2], Wenpeng Wang[3], Huabing Suo[2], Xiaohu Jian[1], Chao Wang[2], Haibo Ma[2], Hong Gao[2,*], Zhaoli Yang[2], Tao Huang[2], Jianmin Ma[1]

Affirmations:

[1] Laboratory for Earth Surface Processes, College of Urban and Environmental Sciences, Peking University, Beijing, 100871, P. R. China

[2] Key Laboratory for Environmental Pollution Prediction and Control, Gansu Province, College of Earth and Environmental Sciences, Lanzhou University, Lanzhou, 730000, P.R. China

[3] College of Atmospheric Sciences, Lanzhou University, Lanzhou, 730000, P.R. China

[*] **Corresponding author:** Xiaodong Zhang, email: zhangxd2020@pku.edu.cn; Hong Gao, email: honggao@lzu.edu.cn

ABSTRACT:

Previous studies have shown that surface air temperature (SAT) facilitates the formation of surface ozone (O_3), while relative humidity (RH) often inhibits ozone generation. However, the degree to which O_3 may respond simultaneously to rising SATs and RH due to climate change remains less understood. We conducted extensive atmospheric chemistry model scenario simulations to investigate the impacts of long-term trends of humidification and warming on summer O_3 concentrations in Northwestern China (NW) from 1998 to 2017, a period during which this region experienced both warming and the most significant wetting trend in China. We found that the summer mean O_3 level in NW increased by 19.9% during this time. The changes in meteorology led to a reduction in O_3 levels, primarily due to humidification in NW, which counteracts the warming-induced O_3 increase. We demonstrate that the wetting trend in NW will continue from 2019 to 2030 under a shared socioeconomic pathway (SSP) in conjunction with a representative concentration pathway SSP5-RCP8.5, but will either cease or shift to drier conditions from 2019 to 2060 under the SSP2-RCP4.5. No significant responses of O_3 fluctuations to RH variations were observed, partly due to manual intervention under the SSP2-RCP4.5.

Keywords: Ozone, Wetting, Warming, Northwestern China, Future projection

1. Introduction

Atmospheric humidity is recognized as a crucial factor that directly and indirectly influences the formation and evolution of surface ozone (Ghazali et al., 2022; Han et al., 2011; Kerr et al., 2020). The relationship between atmospheric humidity and surface O_3 is complex. From a chemical standpoint, humidity can modify the rates of photochemical reactions, thereby affecting O_3 formation. Additionally, humidity plays a role in generating hydroxyl radicals (OH) in the atmosphere, which are vital for breaking down volatile organic compounds (VOCs) and other pollutants (Ding et al., 2023; Ma et al., 2021). These radicals can interact with O_3 precursors, impacting the rate of O_3 production. High humidity can also enhance aerosol formation, facilitating heterogeneous reactions. Depending on the specific chemical pathways involved, some of these reactions may either generate or deplete O_3 (Eck et al., 2020). From a physical perspective, humidity is critical for cloud and fog formation as well as precipitation. The latter promotes O_3 dissolution in water droplets and its removal from the atmosphere through wet deposition, particularly during precipitation events, which weakens solar radiation and disrupts the energy balance near the surface (Ding et al., 2021; Eck et al., 2020; Kleeman, 2008; Madden and Williams, 1978; Millstein and Harley, 2009).

It has been reported that O_3 levels increased by 30% over Northern China in summer and 50% over Eastern China in autumn during a dry year compared to a wet year, indicating that wet climate conditions do not support rising O_3 levels (Ding et al., 2023). Long-term ambient O_3 measurement data indicate that rising absolute air humidity resulted in lower near-surface O_3 concentrations at temperatures of 0−30°C (Belan and Savkin, 2019). Other studies examining the relationship between O_3 concentrations and atmospheric humidity have also identified negative correlations between O_3 levels and humidity (Li et al., 2022). Nevertheless, significant knowledge gaps regarding the relationship between humidity and O_3 persist (Li et al., 2021). Most previous studies utilized short-term or instantaneous O_3 concentrations to evaluate the associations between O_3 and atmospheric humidity (Gong et al., 2021; Li et al., 2021). Their long-term relationships still require clarification. Previous investigations of the connections between climate and O_3 primarily focused on the impact of air temperature, which often overshadows the effects of other meteorological variables (Wang et al., 2024). The extent to which atmospheric humidity could significantly influence the long-term O_3 trend remains uncertain, given that the synergistic effects of warming and wetting frequently occur in a warming climate.

62   In recent decades, Northwestern China has emerged as a critical region for studying O_3
63   variability due to its unique climatic and environmental conditions. Observational studies report a
64   significant increase in summer surface O_3 concentrations across the region, with trends ranging
65   from 1.5–3.0 µg m^{-3} yr^{-1} between 2000 and 2020 (Li et al., 2020; Zhang et al., 2022). This rise has
66   been attributed to intensified anthropogenic emissions (e.g., NO_x and VOCs from energy and
67   industrial activities) and shifting meteorological patterns, including the 'warming and wetting'
68   climate regime (Yang et al., 2023). For instance, Ding et al. (2023) identified a 20% increase in
69   O_3 levels during dry years compared to wet years in arid regions, highlighting the sensitivity of O_3
70   to humidity. In this context, O_3 and RH trends in NW over the past decades likely present a unique
71   scenario to help bridge this knowledge gap. NW (Fig. S1), located in the hinterland of the Asian-
72   European continent, is Asia's largest arid and semi-arid region, characterized by limited rainfall
73   and vegetation (Koster et al., 2004; Yang et al., 2023). Meteorological records indicate that from
74   1960 to 2013, precipitation in NW increased at a rate of 0.55 mm per year (Li et al., 2012; Liu et
75   al., 2013; Yang et al., 2017). During this period, the air temperature rose at a rate of 0.034 °C per
76   year, exceeding the warming trends observed across all of China (0.025 °C per year) and globally
77   (0.013 °C per year). Although RH does not exhibit a significant growth trend during this period,
78   in the recent decade (2008-2017), it increased markedly at a slope of 0.313 in NW and 0.381 in
79   the three westernmost provinces of Xinjiang, Gansu, and Qinghai within NW. Based on these
80   records, NW appears to be entering a "warming and wetting" phase, accompanied by a rise in
81   precipitation, runoff, and lake levels (Nie et al., 2022; Peng and Zhou, 2017; Shi et al., 2002; Yao
82   et al., 2021).

83   The present study aims to address the knowledge gap in the complex and long-term
84   relationships between ozone pollution and atmospheric humidity, focusing on NW, where
85   increasing O_3 pollution, air temperature, and humidity have co-occurred (Peng and Zhou, 2017;
86   Yang et al., 2017), mainly since the early 2000s. This research provides valuable insights into the
87   broader context of air quality management and climate variability by enhancing our understanding
88   of the long-term relationship between ozone pollution and atmospheric humidity.

89

90   **2. Method and data**

91   **2.1 WRF-Chem Model Configuration**

92   Since measured O_3 concentration data in China is only available after 2013, we applied the

93   three-dimensional Weather Research and Forecasting with Chemistry (WRF-Chem) version 3.7

94   model (http://www2.mmm.ucar.edu/wrf/users/wrf_files/wrfv3.7/updates-3.7.html) to predict

95   meteorology, O_3 concentrations, and other relevant data in Northwestern and mainland China. The

96   model domain spans the entire mainland China at a 20 km × 20 km resolution, extending vertically

97   from the surface to the lower stratospheric ozone layer at an altitude of 50 hPa with 30 staggered

98   vertical layers. This vertical segmentation facilitates a deepened comprehension of the O_3

99   dynamics within the region, enabling the capture of its detailed behavior throughout the

100   atmospheric stratifications (Li et al., 2020; Zhang et al., 2020, 2022). Detailed physical and

101   chemical schemes contributing to O_3 formation in WRF-Chem and emission input followed

102   previous studies (Bei et al., 2018; Bossioli et al., 2016; Liao et al., 2015; Tie et al., 2009; Wild et

103   al., 2000) and are presented in Section S1 in the Supplement and Tables S1-S2. The soil NO, NO_x,

104   and HONO emissions have been considered a necessary process contributing to surface ozone

105   formation in recent years (Lu et al., 2021). However, given the lack of soil emission inventories

106   of these reactive nitrogen species in China and the world, the present modeling study did not take

107   these processes into consideration. The aerosol feedback mechanisms include the direct and

108   indirect effects, the both are considered in WRF-Chem. The model simulations with a nudging

109   option in WRF were conducted from June 1st to August 31st in each summer from 1998 to 2017,

110   with a time-step of 30s. A spin-up time of three days was adopted before June 1st in each summer.

111   Further details are referred to Section S1 in the Supplement.

112   Located in the upstream of China in terms of dominant prevailing westerly winds in the mid-

113   latitudes of the Northern Hemisphere, it is expected that Northwestern China would receive more

114   O_3 and its precursors from foreign sources in Eurasian countries to the west of China compared to

115   Eastern China (Li et al., 2014; Li et al., 2016). Such "upstream" effect is implicitly accounted for

116   in meteorology and chemistry lateral boundary conditions under an open boundary approach

117   (https://www2.acom.ucar.edu/wrf-chem). These boundary conditions typically come from global

118   chemical transport model outputs (e.g., GEOS-Chem, MOZART) that themselves simulate O_3 on

119   a global scale (including those upstream regions), chemical reactions, wet and dry deposition, and

120   atmospheric transport processes. These datasets are usually generated or assimilated from global

121   models and observations. The lateral boundary conditions govern the fluxes and concentration

122   levels of pollutants entering the model domain from external (upstream) regions. They represent

123 the environmental or regional background concentration outside the model domain, which already

124 integrates emissions and transport influences from a broader region (including upstream areas).

125 The lateral boundary conditions of chemical species in our modeling exercise were estimated from

126 MOZART-4 reanalysis driven fields (Emmons et al., 2010; Zhang et al., 2020) on a daily basis.

127 The ERA-Interim data with a 6-hourly time resolution and $0.7° \times 0.7°$ lat/lon spatial resolution

128 provided by the ECMWF (European Centre for Medium-Range Weather Forecasts) were adopted

129 as lateral boundary conditions of meteorology. Further, since the multiple model scenario

130 simulations in our study used the same lateral boundary conditions, this effectively removed the

131 influences of precursor emissions and atmospheric transport from Eurasian countries but focused

132 on the wetting impact on O_3 evolution in the internal model domain (China).

133 **2.2 Trend**

134 The Mann-Kendall (MK) Test and Sen's slope (El-Shaarawi and Niculescu, 1992; Kendall, 1949;

135 Mann, 1945) were used to examine the trend of O_3, near-surface air temperature (SAT) at the 2m

136 height, and relative humidity (RH, %) at the 2m height. The Mann-Kendall (MK) Test and Sen's

137 Slope are both non-parametric statistical methods commonly used for analyzing trends in time

138 series data. The MK Test helps determine if there is a significant trend, and Sen's slope quantifies

139 the strength and direction of the trend (slope value).

140   Interannual ozone variability in Northwestern China is primarily driven by large-scale

141 meteorological shifts (e.g., warming, humidification) and regional precursor emissions, rather than

142 diurnal processes. Previous studies (Cooper et al., 2014; Li et al., 2020) have revealed that long-

143 term O_3 trends (interannual and interdecadal scales) are robustly represented by seasonal or annual

144 mean concentrations, as diurnal variations associated with daytime photochemistry and nighttime

145 titration are statistically insignificant. For example, Ding et al. (2023) reported that separating

146 daytime and nighttime O_3 yielded negligible differences (>95% correlation) in O_3 trend over a 20-

147 year period in arid seasons in China.

148 **2.3 O_3 Attribution to Meteorology and Emission**

149 We calculated the fraction (percentage change, %) to account for O_3 attribution to meteorology

150 and emission subject to different model scenarios. For example, we define the fraction

151 $F_{O3} = (C_{S3} - C_{S1}) / C_{S1} \times 100\%,$ (1)

152 as the attribution of O_3 concentration to emissions, where C_{S1} and C_{S3} are the summer surface O_3

153 air concentrations from the base (S1) and fixed meteorology (S3) scenarios.

154 **2.4 Data**

155 To initialize and prescribe boundary conditions in the WRF model from 1998 to 2017,

156 meteorological data were sourced from the ERA-Interim reanalysis from the European Centre for

157 Medium-Range Weather Forecast (ECMWF,

158 https://www.ecmwf.int/en/forecasts/datasets/reanalysisdatasets/era-interim). This allows the

159 adoption of the open boundary conditions to dynamically account for cross-regional O_3 and

160 precursor transport, and to resolve both local photochemical production and contributions from

161 transboundary sources, ensuring a comprehensive representation of O_3 dynamics.

162 Anthropogenic emissions were collected from the Emissions Database for Global

163 Atmospheric Research (EDGAR) version 4.3 on a spatial resolution of $0.1° \times 0.1°$, which was

164 available when we started this modeling investigation. A grid-mapping program implemented the

165 emissions into the WRF-Chem (Crippa et al., 2018; Mo et al., 2017). Biogenic emissions were

166 simulated using MEGAN version 2.1 (Guenther et al., 2006, 2012). A recent study suggests that

167 temperature can alter precursor emissions (Pfannerstill et al., 2024). However, since available

168 emission inventories worldwide, including the widely-used EDGAR inventory, did not account

169 for the influence of meteorology, typically the air temperature, on emissions but only considers

170 emissions from anthropogenic and natural sources, the emissions input in the present modeling

171 might be subject to additional uncertainties. The reduction of these uncertainties will depend on

172 improved inventories that take the meteorological effect into account.

173 We have replaced WRF land-use change (LUC) data with Chinese land use/land cover remote

174 sensing monitoring database provided by the Data Center for Resources and Environmental

175 Sciences, Chinese Academy of Sciences (RESDC) (http://www.resdc.cn), which significantly

176 improved China's LUC in our investigation of the effect of urbanization on O_3 pollution in China

177 (Zhang et al., 2022). The new LUC data has a spatial resolution of 1 km $\times$ 1 km, which is

178 extrapolated to the WRF-Chem grid cells (20 km $\times$ 20 km).

179   Considering that the warming and wetting trends in NW might persist in the coming decades,

180   we also projected future O_3 and meteorology in 2019, 2030, and 2060 in the WRF-Chem model

181   framework and simulations, respectively. We collected future anthropogenic emission data from

182   the Dynamic Projection Model for Emissions in China (DPEC Inventory – MEICModel,

183   http://meicmodel.org.cn), with a spatial resolution of $0.25° \times 0.25°$ longitude and latitude (Cheng

184   et al., 2021, 2023; Tong et al., 2020). The meteorological data was collected from Shared

185   Socioeconomic Pathways (SSP) and Representative Concentration Pathways (RCP) climate

186   scenarios under the CMIP6 framework (https://aims2.llnl.gov/search/cmip6/), with the MPI-

187   ESM1-2-HR model (Eyring et al., 2016). Compared with other models, MPI-ESM1-2-HR has

188   higher resolution and can simulate the complex interactions within the climate system, including

189   all climate scenarios (SSP2-RCP4.5 and SSP5-RCP8.5) targeted by this study, and has been widely

190   used in WRF simulations.

2.5 Model Evaluations

192   Rigorous comparisons between simulated O_3 concentrations and measured data were

193   conducted and presented in Figs. S2-S7 and Section S2 in the Supplement. Overall, the simulated

194   O_3 concentrations agree reasonably well with measured data, demonstrating a high level of

195   reliability of modeling results.

2.6 Model Scenario Setup

197   We established several model scenarios to distill signals of meteorological conditions, primarily

198   SAT and RH, in modeled O_3 concentrations. Detailed configurations are provided in Table 1. The

199   first scenario (S1) serves as the baseline, incorporating summer-specific meteorological variables

200   and emissions from 1998 to 2017 into WRF-Chem simulations, and is thus considered a realistic

201   scenario. In the second scenario (S2), we fixed emissions from 1998 throughout the period from

202   1998 to 2017, aiming to assess the significance of the meteorological effect on O_3 variation. In the

203   third scenario (S3), we fixed meteorology from 1998 during the same period, thereby emphasizing

204   the importance of emissions in O_3 variation. To evaluate the sensitivity of scenario S3, we also

205   conducted an additional WRF-Chem run by fixing SAT and RH only in 1998 (scenario S4) and

206   compared the modeled O_3 concentrations with those simulated in scenario S3 for 2004. Overall,

207   we found minor differences (two tails T-test = 0.1065) between model scenario S3 and the results

208   from the fixed SAT and RH model run (Fig. S8) but slightly stronger O_3 pollutions subject to fixed

209   RH and SAT scenario than S3 results can be discerned in the Northern China Plain. ozone

210   concentrations under fixed SAT and RH in 1998 seemed higher than fixed all meteorology in 1998

211   (S3 scenario). We further calculated the differences of the planetary boundary layer heights (PBLH)

212   between the two scenarios (fixed RH and SAT scenario minus scenario S3). The results are

213   illustrated in Fig. S9. Negative PBLH differences can be seen in many areas across China,

214   including the NCP, indicating that fixed SAT and RH scenario reduced PBLH, which often

215   associates with stronger air pollution within the PBLH. By calculating the differences and fractions,

216   we can discern the contributions of meteorology and emissions to O_3 formation and destruction.

217   We also established two additional model scenarios to project the responses of O_3 concentrations

218   to future meteorology and emissions in NW based on CMIP6 pathways SSP2-RCP4.5 and SSP5-

219   RCP8.5, specifically for 2019, 2030, and 2060, respectively. Detailed descriptions of these two

220   pathways and the corresponding data are presented in Section S3 in the Supplement.

221

222   **Table 1.** Model scenarios.

Scenario	Simulation period	Meteorology	Emission	LUC
S1	1998-2017	Varied	Varied	Varied
S2	1998-2017	Varied	Fixed (1998)	Varied
S3	1998-2017	Fixed (1998)	Varied	Varied
S4	2004	Only fixed SAT and RH (1998)	Varied	Varied
S5	1998-2017	Varied	Varied	Fixed (1998)
SSP2-4.5	2019, 2030, 2060	Varied	Varied	Varied
SSP5-8.5	2019, 2030, 2060	Varied	Varied	Varied

223

3. Results and Discussion

3.1 Summer Ozone Trends

226   Figures 1a and 1b present MK-Test statistics and Sen's slope estimated temporal trends of summer

227   O_3 concentrations from 1998 to 2017 under scenario S1 (base scenario) and S3 with fixed

228   meteorology in China. In the S1 scenario (Fig. 1a), O_3 concentrations exhibit statistically

229   significant declining trends in the northernmost regions, spanning from Northeastern Xinjiang to

230   Northeastern China, with the most significant decline occurring in Inner Mongolia. Increasing O_3

231   concentrations are observed along Tianshan Mountain in Xinjiang, western Tibet, and central

232   China. The fixed meteorology scenario (S3, Fig. 1b) shows a monotonically increasing trend

233   across China, indicating continuously rising O_3 levels for the past two decades due to growing

234   precursor emissions, except for some grid cells in the Yangtze River Delta (YRD), the Pearl River

235   Delta (PRD), the Beijing-Tianjin metropolitan area, and other sporadic regions, where MK-Test

236   and Sen's slope identified statistically significant negative O_3 trends. Previous studies have also

237   noted the negative trends over the past decade in these regions (Hu et al., 2024; Li et al., 2022;

238   Wang et al., 2020; Yu et al., 2021). The Beijing-Tianjin area, YRD, and PRD are three critical

239   regions under China's joint efforts to prevent and control air pollution. Regional emission

240   mitigation in these areas may lead to varying reductions in precursor emissions and declines in O_3

241   concentrations. Overall, increasing precursor emissions have dominated the O_3 trend in China, as

242   meteorology remained constant during this period. This is evidenced by the linear trends of NO_x

243   and NMVOC (Non-methane VOC) emissions in China from 1998 to 2017 (Fig. S10). When

244   comparing the MK-Test and Sen's slope results between the two scenarios model runs (Fig. 1c),

245   the meteorological conditions from 1998 to 2017 overshadowed the effects of emissions, primarily

246   contributing to the declining O_3 levels (negative trends) in the northernmost regions of China,

247   extending from Inner Mongolia to Northeastern China. Our modeling result shows that mean

248   summer O_3 concentration averaged over Inner Mongolia reached the maximum in 2007 and

249   slightly declined thereafter (Fig. S11). This can be partly attributed to relatively lower precursor

250   emissions resulting from the sparse population and limited industrial activities in this part of China,

251   though having a growing trend (Zhang et al., 2022, 2023).

252
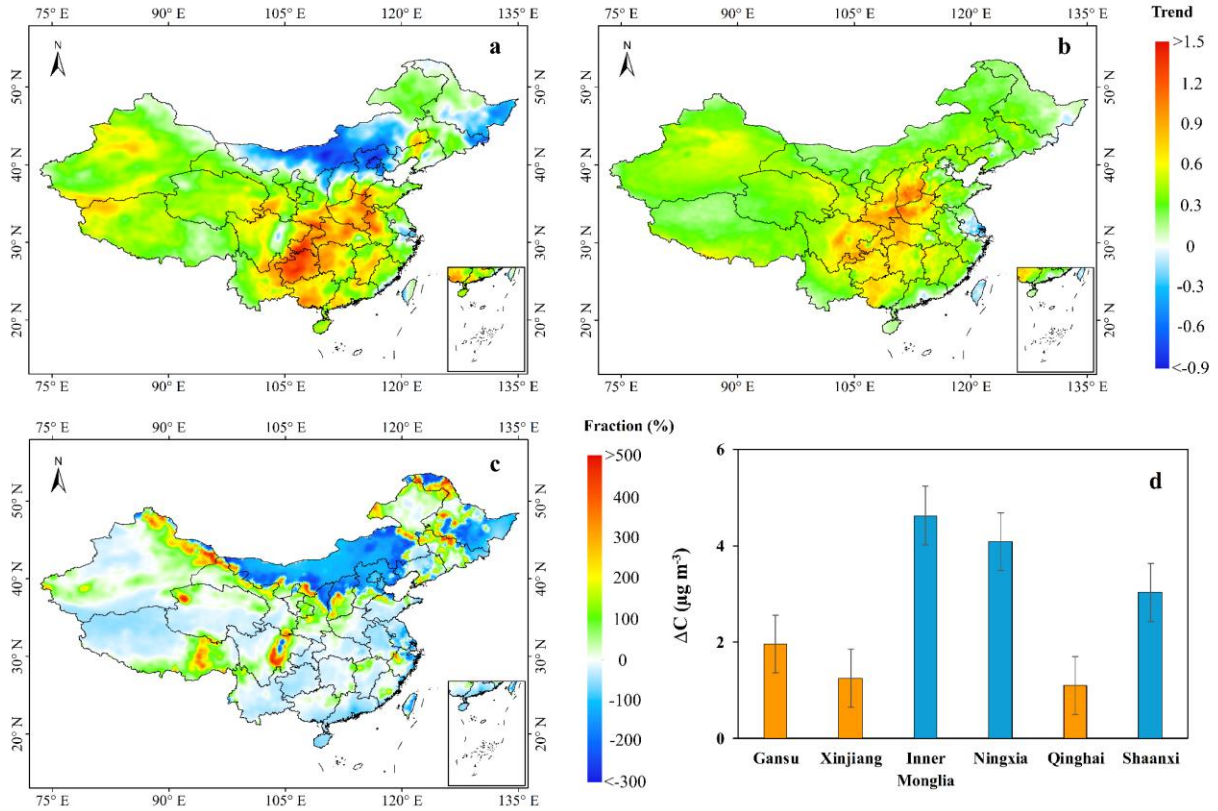
Figure 1. MK-Test and Sen's slope estimated summer O_3 concentration trend and O_3 attribution (fraction or percentage change, %) under baseline (S1) and fixed meteorology (S3) scenarios from 1998 to 2017, respectively. (a) MK-Test and Sen's slope estimated trend from the base scenario S1, the trends of concentrations are well within the MK-Test statistically significant range at 95% confidence level in terms of |Z|>1.96 criteria; (b) same as Fig. 1a but for fixed meteorology scenario S3; (c) fraction of O_3 concentration trend between the model scenarios 1 and 3 from 1998 to 2017; (d) mean differences of summer mean O_3 concentrations averaged from 1998 to 2017 between the model scenarios 1 and 3, defined by $\overline{\Delta O_3} = \bar{O}_{3,S1} - \bar{O}_{3,S3}$, where $\bar{O}_{3,S1}$ and $\bar{O}_{3,S3}$ stand for mean summer O_3 concentrations averaged over 1998 to 2017, respectively. $\overline{\Delta O_3}$ in three Westernmost provinces of NW is shown by yellow bars and blue bars for three Easternmost provinces of NW. Error bar in Fig. 1d stands for ±1 STD.

To discern potential influences of meteorology on O_3 concentrations at the provincial level, we estimated the differences of summer mean O_3 concentrations averaged from 1998 to 2017 between model scenarios 1 (S1) and 3 (S3), defined by $\overline{\Delta O_3} = \bar{O}_{3,S1} - \bar{O}_{3,S3}$. Figure 1d illustrates $\overline{\Delta O_3}$ in each province of Northwestern China. Since the mean O_3 levels under scenario S1 were greater than those under scenario S3 with fixed meteorology in 1998, although in some years we also identified negative ΔO_3 in the three westernmost provinces (Xinjiang, Gansu, and Qinghai), we would expect positive $\overline{\Delta O_3}$, as shown in Fig. 1d. In this context, the values of $\overline{\Delta O_3}$ indicate the

270   extent of meteorological influence on O_3 concentrations. Specifically, the smaller $\overline{\Delta O_3}$, the

271   stronger meteorological influences, as a smaller $\overline{\Delta O_3}$ suggests that O_3 levels with varying

272   meteorology (S1) are closer to those with fixed meteorology in 1998 (S3). We highlighted the

273   three provinces with smaller $\overline{\Delta O_3}$ (<2 μg m^{-3}) using yellow bars, all located in Westernmost NW,

274   indicating a weaker increase in O_3 concentrations in these three westernmost provinces compared

275   to others, aligning well with the RH trends in these provinces, as compared to the other three

276   provinces located in the east of NW (Inner Mongolia, Ningxia, and Shaanxi), as mentioned in the

277   Introduction. As shown in Fig. S12, modeled concentration fractions under the S2 model scenario

278   with fixed emissions in 1998 in the three westernmost provinces of NW are negative, indicating

279   that meteorology tended to inhibit the increase in summer ozone concentrations, particularly in

280   Xinjiang, Gansu, and Qinghai, confirming the result in Fig. 1d. In the other three provinces to the

281   east of NW, we observe larger $\overline{\Delta O_3}$ values, suggesting that meteorology, along with precursor

282   emissions, tended to enhance O_3 levels from 1998 to 2017. Consequently, we would expect that

283   meteorology favored O_3 growth in these three eastern provinces of NW.

284   **3.2 Associations of summer ozone with wetting and warming**

285
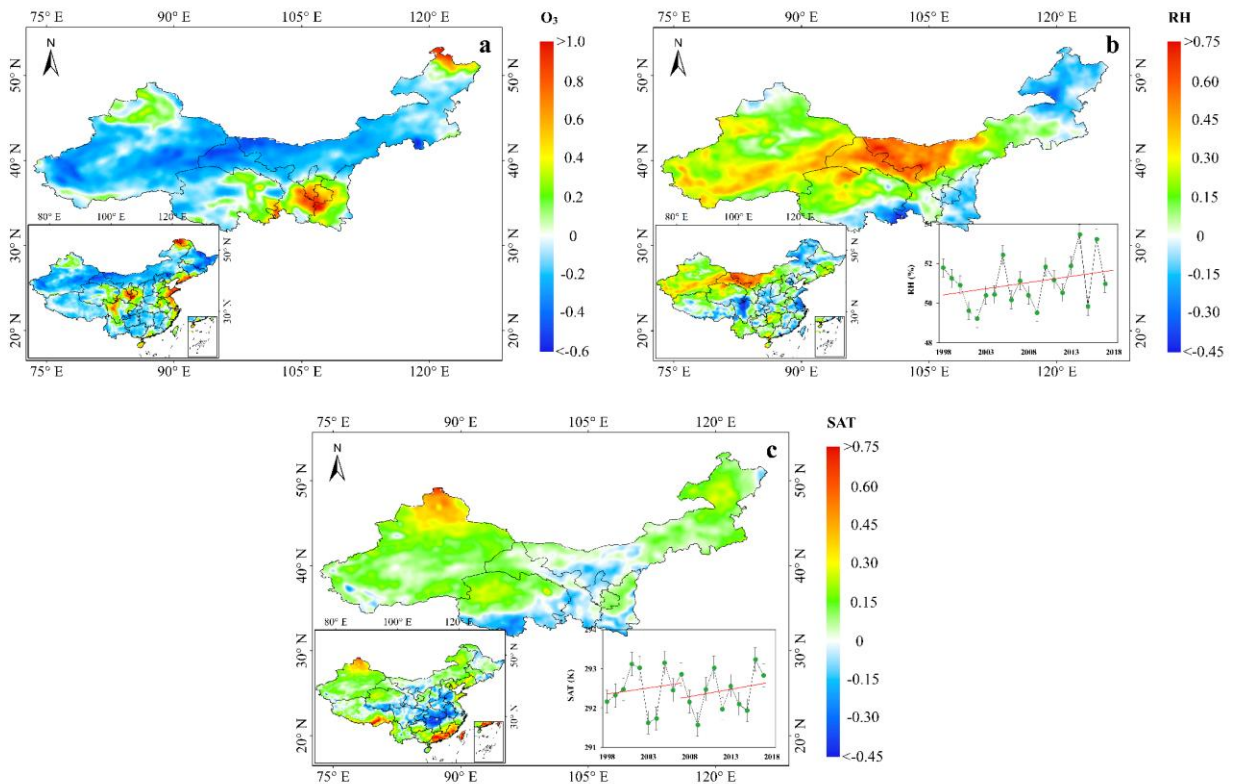
286 **Figure 2.** (a) MK-Test statistics for the trends of summer O_3 concentrations from 1998 to 2017 subject to model
287 scenario 2 (S2) with fixed emissions in 1998, (b) MK-Test statistics for summer RH from 1998 to 2017, the line
288 chart on the low-right corner illustrates summer RH in NW from 1998 to 2017 under scenario 2, (c) MK-Test
289 statistics for trend of summer SATs from 1998 to 2017, the line chart shows summer SATs averaged over
290 Northwest China from 1998 to 2017, under scenario 2. Contour figures on the low left corner of Figs. 2a-2c
291 illustrates MK-Test statistics for O_3 trends under fixed emission (model scenario 2) and modeled RH and SAT
292 trends in mainland China from 1998 to 2017. The trends are well within the statistically significant range at 95%
293 confidence level in terms of |Z|>1.96 criteria.

294   Figure 2a illustrates the MK-Test statistics of gridded summer O_3 concentrations from 1998

295 to 2017 subject to the model scenario S2 with fixed emissions and annually varied meteorology,

296 aiming to highlight the effect of meteorology on O_3 evolution. A notable decline in summer O_3

297 ozone concentrations is evident in most areas of mainland China, except for the Northern China

298 Plain, central China, the Sichuan Basin, and the Guanzhong Plain (inner figure on the left-low

299 corner of Fig. 2a). The declining O_3 trends are also evident in most regions across NW with the

300 most substantial decrease occurring in west Gansu, northwest Inner Mongolia, and Xinjiang. With

301 fixed emission, such an O_3 falling trend is induced primarily by meteorology (climate).

302 Considering that air temperature and humidity are two key meteorological factors influencing O_3

303 fluctuations, we present the MK-Test statistics of the trends of summer relative humidity (RH, %)

304 at the 2 m height in Northwestern and mainland China (illustrated in the lower-left corner of Fig.

305 2b), along with their annual variations depicted in a line chart in the lower-right corner of Fig. 2b.

306 We also present the surface air temperature (SAT, K) in Northwestern and mainland China in a

307 line chart in the lower-right corner of Fig. 2c. Compared to many places across Eastern and Central

308 China where RH has negative or drying trends (left-low corner of Fig. 2b), RH in NW showed a

309 marked surge, suggesting pronounced wetting, as reported before (Peng and Zhou, 2017). This can

310 also be seen in the annual changes in the mean RH averaged over NW (the line chart on the right-

311 low corner of Fig. 2b) from 1998 to 2017, dominated by an overall upward RH trend with a mean

312 growth rate of 1.9% per year. Likewise, NW also experienced warming during the same period, as

313 shown in Fig. 2c, particularly in the western part of NW, including Xinjiang, western Gansu

314 Province, and Qinghai Province. NW has been undergoing one of the most significant warming

315 trends in the nation. Between 2005 and 2017, NW, particularly the Xinjiang region, has warmed

316 by over 0.5 K with a rate of 0.04 K/yr. In contrast, eastern and Central China show a cooling trend.

317 The rising SAT trend and falling O_3 trend are in contrast to the common knowledge that increasing

318 SATs should enhance O₃ levels. The result thus implies that SATs did not dominate the O₃ trend

319 in NW.

320

321
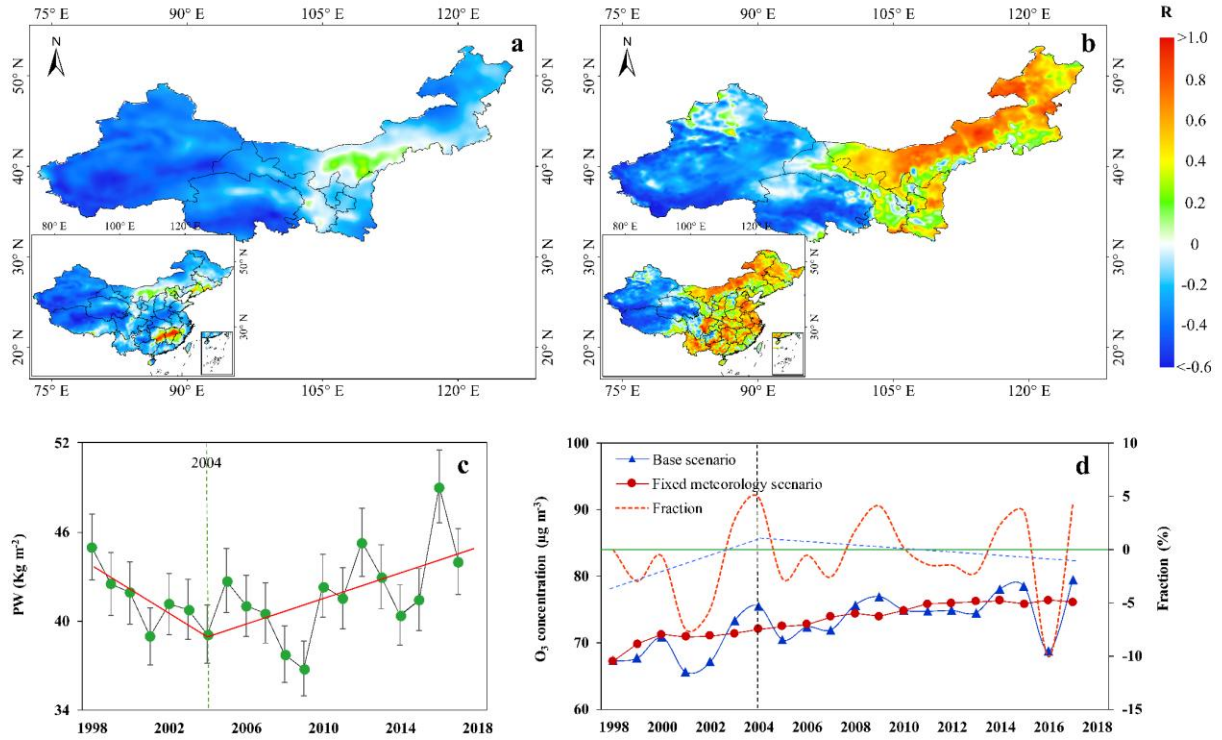
Figure 3. (a) Pearson correlation (R) between summer O_3 concentration and RH from 1998 to 2017 under S2
scenario, (b) R between summer OH radical concentration and O_3 concentration from 1998 to 2017 under S2
scenario, (c) summer surface precipitable water (PW) in the bounded area of NW from 1998 to 2017, error bar
stands for ±1 STD and red solid line stands for linear trend, (d) summer O_3 concentrations under Scenarios 1
(dark blue solid line with triangles) and 3 (red solid line with circles) scaled on the left-Y axis, and their fractions
$F_{O3} = (C_{S1} - C_{S3}) / C_{S3} \times 100\%$ (red dashed line) in three Westernmost provinces of HW (Xinjiang, Qinghai,
and Gansu), where C_{S1} and C_{S3} are the summer (June to August) surface O_3 air concentrations from the base (S1)
and fixed meteorology (S3) scenarios, scaled on the right-Y axis, the blue dashed line in Fig. 3d is a linear fitting
line from 1998 to 2004 and 2004 to 2017, respectively. The green solid line represents the zero-value line of the
fraction.

332   As mentioned earlier, since rising temperatures favor O_3 formation while increasing humidity

333 is detrimental to O_3 growth, it is intriguing to investigate which of these two meteorological factors

334 contributes more to the O_3 trend in NW. We first calculated linear correlation coefficients between

335 RH and O_3 concentrations modeled from the S2 scenario (fixed emissions) from 1998 to 2017

336 across Northwestern and mainland China (bottom left corner of Fig. 3a). Strong negative

337 correlations are evident in most regions of Xinjiang, Qinghai, and Western Gansu. These negative

338 correlations indicate declining O_3 concentrations with rising RH. To highlight the influences of

339 RH and precipitation on summer O_3 variation, Fig. 3d illustrates modeled mean summer O_3

340 concentrations averaged over three Westernmost provinces of HW (Xinjiang, Qinghai, and Gansu)

341 under the base scenario S1 with annually varying summer meteorology and emissions, and S3 with

342 fixed meteorology in 1998 and annually varying emissions averaged over NW, along with the

343 concentration fractions (%, red dashed line) between the two scenarios from 1998 to 2017. O_3

344 concentrations exhibit the same increasing trend primarily driven by rising precursor emissions.

345 However, the S1 scenario shows more significant annual fluctuations (solid dark blue line in Fig.

346 3d) compared to the S3 scenario (solid red line in Fig. 3d). These stronger fluctuations can be

347 attributed to the influence of meteorology. Since scenarios 1 and 3 shared the same emissions and

348 chemistry, the concentration fractions quantify the contributions of meteorology to the O_3 trend

349 alone. As shown, the fractions increased from 1998 to 2004, decreased thereafter, and turned

350 negative since 2009 (the red dashed lines), indicating that meteorology has led to declining O_3

351 concentrations since 2005 in NW. Among the two key meteorological factors influencing O_3

352 formation, increasing SAT (Fig. 2c) tends to elevate O_3 levels, which contradicts the decreasing

353 and negative O_3 fractions. Consequently, RH likely plays a more significant role in the O_3 trend in

354 NW, as rising RH aligns well with the decreasing and negative O_3 fractions.

355 Figure 3c displays the mean summer surface precipitable water (PW, kg/m2) over the region

356 bounded between 75 – 100°E in Northwest China from 1998 to 2017, collected from the NCAR

357 reanalysis (https://psl.noaa.gov/cgi-bin/data/composites/printpage.pl). One can identify a slow

358 decrease in PW from 1998 to 2004 and a rapidly growing PW thereafter. Since warming

359 exacerbates drought in arid and sub-arid NW (Lian et al., 2021), growing precipitation in NW

360 implies that increasing humidity might play a more significant role than warming in the changing

361 climate, which acts to reduce O_3 levels via precipitation washout and chemistry. A close look at

362 Figs. 2b, 2c, and Fig. 3a indicate that more substantial warming and wetting occurred in Xinjiang,

363 Gansu (including westernmost of Inner Mongolia), and Qinghai provinces. We compared the

364 fractions of provincial mean summer RH and summer O_3 concentrations from the fixed emissions

365 and annually varying meteorology scenario (S2) between 1998 and 2017 (Fig. 4a), defined by $f =$

366 $(Y_{2017} - Y_{1998}) / Y_{1998} \times 100\%$, where f is the concentration or RH fractions and Y_{1998} and Y_{2017} stand

367 for O_3 concentrations or RH in 1998 and 2017, respectively, thereby to highlight the net effect

368 from meteorology. The most significant fraction of O_3 concentration was identified in Inner
369 Mongolia at 9.9%, followed by Ningxia (5.7%), Shaanxi (5.5%), Gansu (2.8%), Xinjiang (1.6%),
370 and Qinghai (-1.5%), respectively. Among the six provinces, Xinjiang and Gansu accounted for
371 smaller O_3 fractions, and Qinghai accounted for a negative fraction (Fig. 4a), indicating that O_3
372 levels in these three provinces inclined less significantly or even declined (Qinghai) between 1998
373 and 2017 than the other three provinces. Interestingly, more significant O_3 fractions, meaning
374 growing O_3 levels for the two decades in Inner Mongolia, Ningxia, and Shaanxi, correspond to
375 smaller (Ningxia) or negative (Inner Mongolia and Shaanxi) RH fractions, meaning falling RH. In
376 contrast, more diminutive and negative O_3 fractions in Xinjiang, Gansu, and Qinghai provinces
377 are associated well with the stronger increasing trend of summer RH by MK-test (Figs. 2b and 4a)
378 at the growing rate of 9.8% in Xinjiang, 8.9% in Gansu, and 9.9% in Qinghai from 1998 to 2017,
379 respectively. While the weak or falling summer O_3 levels in three provinces respond to both
380 growing RH and SAT trends (Fig. 2b and 2c), since growing SATs tend to enhance O_3
381 concentrations but modeled O_3 respond weakly to rising SAT in these three provinces, the result
382 demonstrates again that the wetting might inhibit O_3 formation and increment for the past decades
383 in NW.

384
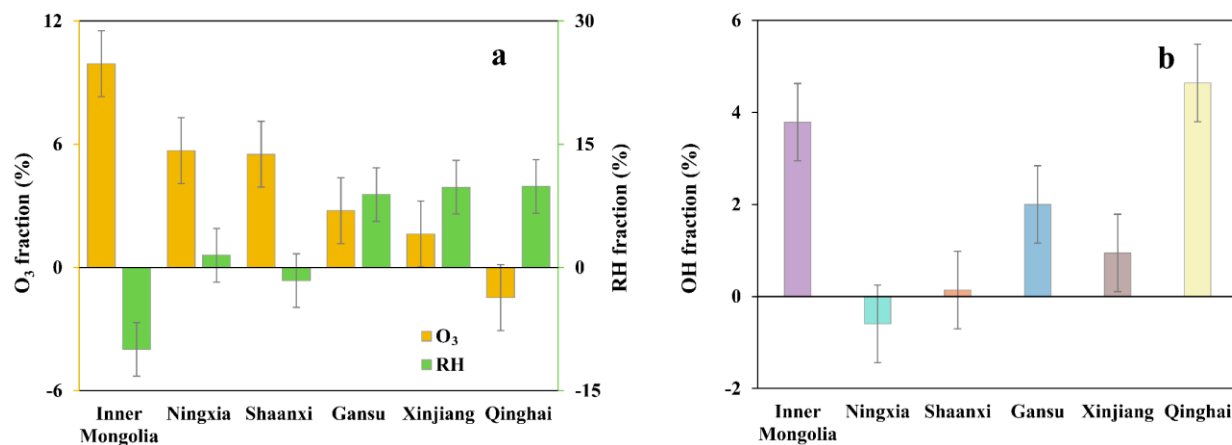
386 **Figure 4.** Summer RH, O_3, and OH radical fractions between 1998 and 2017 in six provinces of NW under the
387 fixed emission scenario (S2). (a) RH and O_3 fractions, O_3 fractions are scaled on the left Y-axis, and RH fractions
388 are scaled on the right Y-axis, (b) OH radical fractions. Error bars denote ±1 STD.

389 It is worthwhile to point out that model scenario 2 with fixed emissions also considers
390 chemistry, in which OH radicals and water vapor can interact. The primary source of OH radicals

391   in the atmosphere is the reaction between water vapor (H_2O) and excited oxygen atoms ($O(^1D)$),

392   which are formed by the photolysis of ozone (O_3) by ultraviolet (UV) radiation. The OH radicals

393   react with ozone to form oxygen (O_2) and the excited oxygen atom $O(^1D)$, which can further react

394   with water vapor to regenerate two OH radicals:

395         $O_3 + OH \rightarrow O_2 + O(^1D)$,

396         $O(^1D) + H_2O \rightarrow 2\ OH.$ (2)
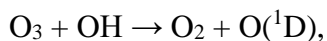
397   This reaction does not lead to a net reduction in OH radicals but contributes to ozone removal by

398   initiating reactions that lead to the formation of less reactive species. Figure 3b is a correlation

399   diagram between modeled summer O_3 concentrations and OH radicals in NW and mainland China

400   (the left-low corner of Fig. 3b) subject to the fixed emission scenario (S2). The spatial pattern of

401   correlation coefficients in NW is, to some extent, similar to that between O_3 concentrations and

402   RH (Fig. 3a), showing the negative associations between OH radicals and O_3 concentrations,

403   particularly in Xinjiang and Qinghai with the most significant wetting trend, suggesting that

404   increasing OH radicals reduce O_3 levels. Figure 4b displays the fractions of provincial mean

405   summer OH radicals from the fixed emissions and annually varying meteorology scenario (S2)

406   between 1998 and 2017. Relatively larger positive fractions can be discerned in Xinjiang, Qinghai,

407   and Gansu, meaning increasing OH radicals in these provinces as a result of increasing RH (Eq.

408   1), which corresponds to higher RH fractions and lower O_3 fractions. An exception occurs in Inner

409   Mongolia, where the large positive OH radical fraction (Fig. 4b) is associated with negative RH

410   and large O_3 fractions (Fig. 4a). OH radicals show an increasing trend (Fig. S13) which agrees

411   with the positive correlation between OH and O_3 concentrations shown in Fig. 3b. This puzzling

412   from the modeling results needs further investigations.

413   There are several primary mechanisms of OH radicals leading to O_3 reduction, including the

414   reaction with VOCs to form peroxyl radicals (RO_2), the reaction of RO_2 with nitrogen oxides (NO_x

415    $= NO + NO_2$) to form nitrogen dioxide (NO_2) and other compounds, and photodissociation of NO_2.

416   Figures S10a and S10b show the MK test estimated NO_x and NMVOC emission trends from 1998

417   to 2017. While increasing NO_x is observed in NW (Fig. S10a), its emission levels are considerably

418   lower than in Eastern and Southern China (Fig. S10c). Both NMVOC emission levels and trends

419   in NW are significantly smaller than in Eastern and Southern China due to lower populations and

420 less developed economies (Fig. S10b and S10d). Hence, it is likely that the reaction of water vapor

421 (H_2O) with excited oxygen atoms ($O(^1D)$) produced by the photodissociation of ozone by UV light

422 plays a specific role in the negative correlation between O_3 and OH radicals.

423   A multiple regression model (MRM) was established to further quantitatively assess the

424 contribution of RH and SAT to summer O_3 concentrations in NW. The MRM has been applied in

425 a number of investigations to quantify meteorological effects on ozone evolution in China (Li et

426 al., 2019, 2020, 2021; Yan et al., 2024). For SAT and RH, the MRM model can be defined as

427     $\ln(O_3) = \alpha + \beta_1 \ln(SAT) + \beta_2 \ln(RH) + \varepsilon,$ (3)

428 where α, β_1, and β_2 are model coefficients, and ε is a random error, respectively. In the first instance,

429 we considered three provinces with significant wetting trends: Xinjiang, Gansu, and Qinghai. We

430 combined annual summer O_3, RH, and SAT from three provinces into one time series of each

431 dependent and independent variable from 1998 to 2017, yielding 60 samples for each variable.

432 Tables S4-S6 present regression coefficients and statistics of the MRM. To examine the

433 multicollinearity in the MRM, we estimated the variance inflation factor (VIF, Table S4-S6). The

434 VIFs for RH and SAT are far less than 10, indicating no multicollinearity in the model. The

435 contribution of RH and SAT to O_3 is calculated by:

436     $\text{Contribution}_i = \dfrac{\left|\beta_i \times \frac{STD_i}{STD_\alpha}\right|}{\text{SUM}},$ (4)

437 where $\text{SUM} = \sum_i |\beta_i \times STD_i/STD_\alpha|$, and β_i denotes the regression coefficient of independent

438 variable i (namely, RH and SAT), STD_i is the standard deviation of regression coefficient of

439 independent variable i, and STD_α represents the standard deviation of coefficient of intercept.

440   The MRM analysis reveals that RH contributes 77.5%, 59.4%, and 46.2% to O_3 variations in

441 Xinjiang, Qinghai, and Gansu. Accordingly, SAT contributes 22.5%, 40.6%, and 53.8% to O_3

442 fluctuations in these three provinces from 1998 to 2017. The results indicate that RH has become

443 a major contributor to long-term change in O_3 concentrations, overwhelming or equivalent to

444 SAT's contributions to the O_3 trend for the past two decades, likely via interactions among

445 increasing precipitation washout and OH radical, O_3 concentration, and water vapor.

446   We further assess the contributions of precipitation, RH, SAT, winds, and PBLH (planetary

447 boundary-layer height) to O_3 evolution in NW using an extended MRM model. The results confirm

448   that RH and SAT made the most significant contributions to long-term ozone trends than other

449   meteorological variables under the long-term perspective. As seen from Fig. 5, the contribution of

450   RH (49.5%) and SAT (47.6%) to O_3 evolution in NW was almost equivalent (Fig. 5a), but the

451   SAT (92.4%) dominated in entire mainland China (Fig. 5b). Whereas the PBLH only contributed

452   about 2% to O_3 variations because the PBLH varies on a daily and hourly basis and affects

453   insignificantly (summer) seasonal changes in O_3 concentrations.

454

455
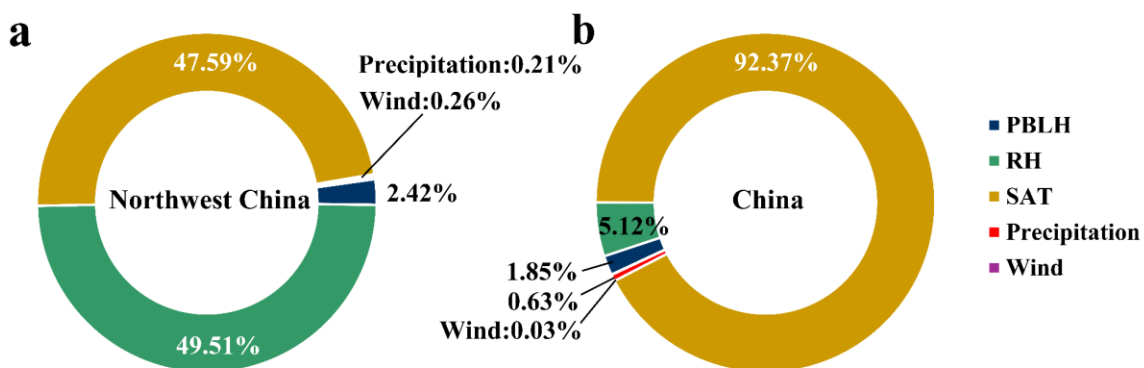
456   **Figure 5.** Contribution of PBLH (planetary boundary-layer height), RH, SAT, precipitation, and wind to O_3
457   evolution. (a) Northwest China, (b). Mainland China.

458   It should be pointed out that since the wetness also helps growing vegetation, which causes

459   increasing biogenic VOC emission (BVOC) and hence rising O_3 concentrations, the contribution

460   of BVOCs to O_3 fluctuations under increasing wetness should also be taken into consideration. To

461   examine this hypothesis, we designed an extra model scenario (S5) in which we used the updated

462   LUC data (section 2.4) and fixed LUC in 1998 in the WRF-Chem simulation and ran the model

463   from 1998 to 2017. Since the LUC defines vegetation coverage, the fixed LUC suggests no

464   vegetation change during this period. We then estimated the fractions between modeled O_3

465   concentration with fixed LUC and the baseline scenario S1 with annually-varying LUC, thereby

466   eliminating the effects from emissions, meteorology, and chemistry but highlighting the LUC (or

467   greenness) effect only. The result is illustrated in Fig. S14. As shown, while the fraction fluctuates

468   positively (Xinjiang) and negatively (Northern Shaanxi and Eastern Inner Mongolia), indicating

469   increasing and decreasing O_3 levels induced by LUC or greening, the magnitudes of provincial

470   mean concentration fractions are very small, mostly ranging from -1% to 0.3%, suggesting that

471   the LUC under the wetting trend in NW plays an insignificant role in O_3 fluctuation.

472   **3.3 Projected future climate impacts on summer Ozone**

473   Given the significant impacts of wetting on O_3 evolution in NW over the past two decades,

474   concerns have also been raised regarding O_3 responses to future wetting and warming. We

475   estimated the projected O_3 concentrations, RH, and SAT fractions between the baseline and fixed

476   meteorology scenarios under the SSP2-4.5 and SSP5-8.5 pathways (section 2.6) for the years 2019,

477   2030, and 2060, respectively (Figs. 6 and 7). As mentioned earlier, since both scenarios

478   implemented the same emissions and chemistry but the baseline scenario accounted for variable

479   meteorology, the fractions (or differences) between the two scenarios eliminated the effects of

480   emissions and chemistry, thereby isolating meteorological signals only.

481
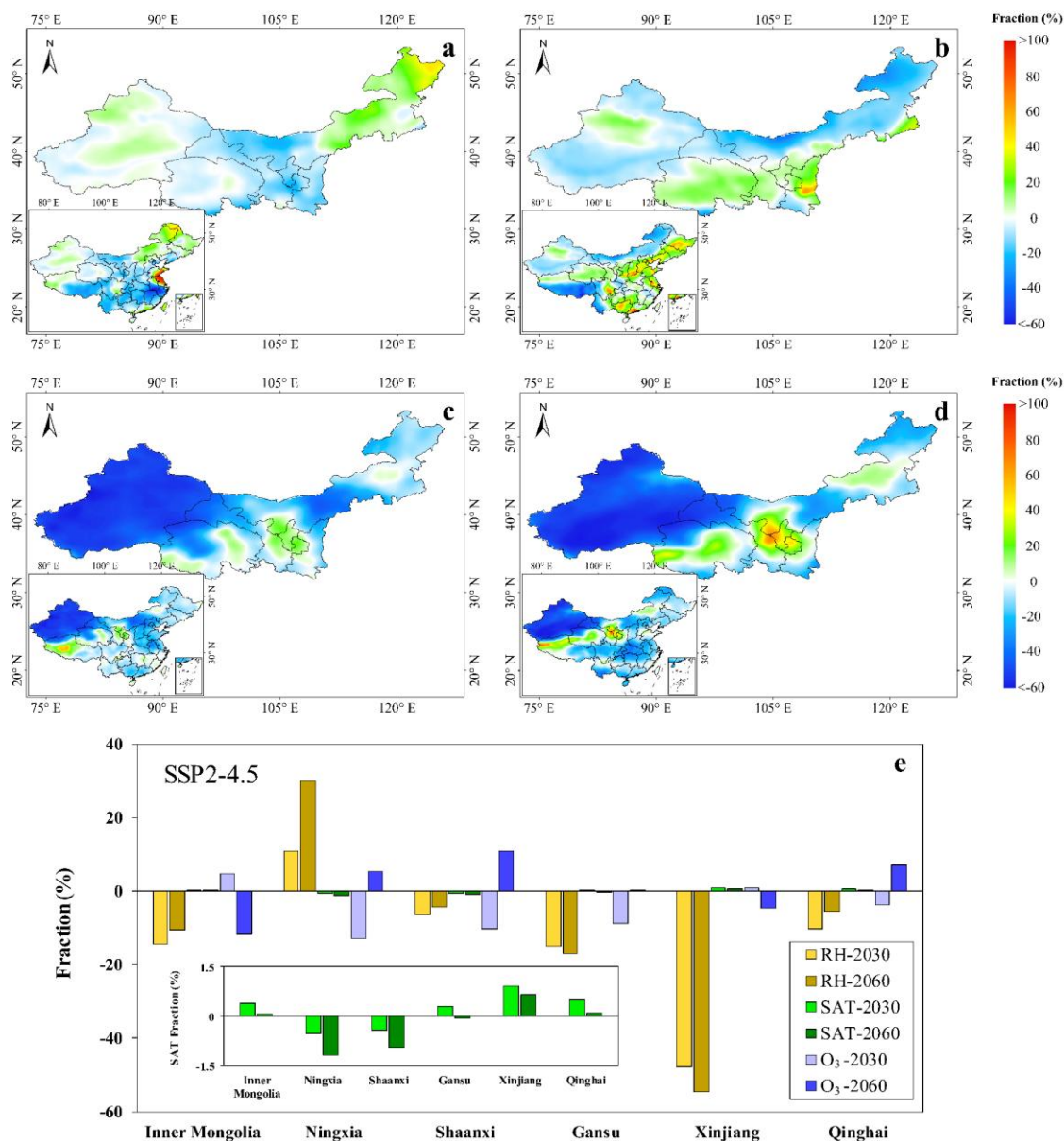
Figure 6. (a) Summer O_3 concentration fractions of 2019 to 2030 under SSP2-4.5scenario, estimated by F_{SSP245} $= (C_{2030} - C_{2019}) / C_{2019} \times 100\%$, where C_{2019} and C_{2030} are the summer surface O_3 air concentrations in 2019 and 2030, respectively, (b) same as Fig. 6a but for O_3 fractions of 2019 to 2060, (c) same as Fig. 6a but for summer RH fractions of 2019 to 2030, (d) same as Fig. 6a but for summer RH fractions of 2019 to 2060, (e) fractions of RH, SAT, and O_3 of 2019 to 2030 and 2019 to 2060 (shown in the same color bar as 2030 but with oblique lines*) in the six provinces of Northwestern China under the SSP2-4.5 scenario.

488
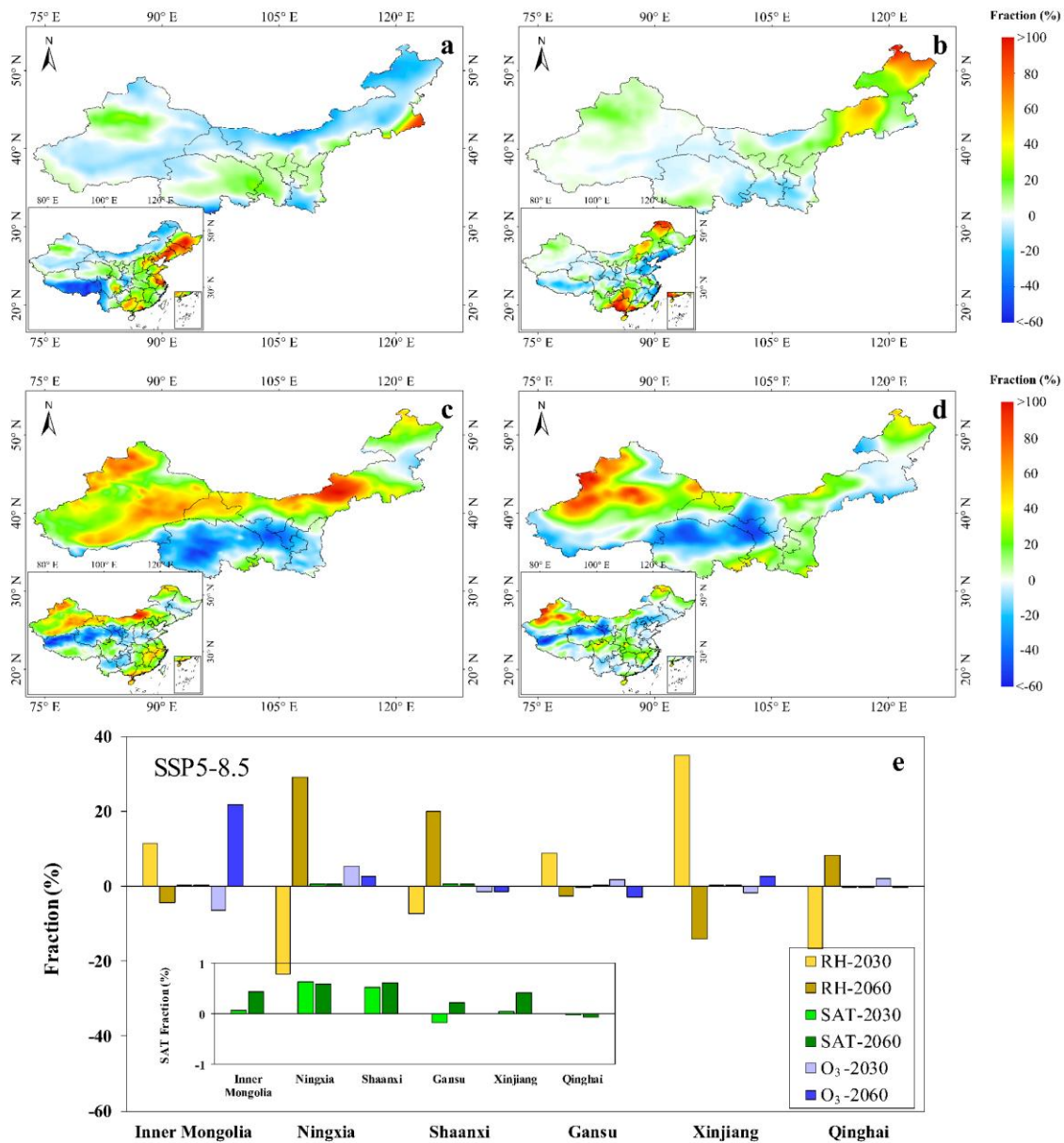
Figure 7. (a) Summer O_3 concentration fraction of 2019 to 2030 under the SSP5-8.5 scenario, estimated by $F_{SSP585} = (C_{2030} - C_{2019}) / C_{2019} \times 100\%$, where C_{2019} and C_{2030} are the summer surface O_3 air concentrations in 2019 and 2030, respectively, (b) same as Fig. 7a but for O_3 fraction of 2019 to 2060, (c) same as Fig. 7a but for summer RH fraction of 2019 to 2030, (d) same as Fig. 7a but for summer RH fraction of 2019 to 2060, (e) fractions of RH, SAT, and O_3 of 2019 to 2030 and 2019 to 2060 (shown in the same color bar as 2030 but with oblique lines) in the six provinces of Northwestern China under the SSP5-8.5 scenario.

Detailed discussions on the associations between projected O_3 evolution and trends of RH and SAT under the SSP2-4.5 and SSP5-8.5 pathways from 2019 to 2030 and from 2019 to 2060 are presented in Section S4 in the Supplement and Figs. 6-7 and Fig. S15, respectively. Overall,

498   from 2019 to 2030, we observe a stronger negative association between O_3 and RH under SSP5-
499   8.5 than under SSP2-4.5 across NW, suggesting that climate conditions under the SSP5-8.5
500   scenario will more effectively suppress O_3 growth compared to SSP2-4.5 during this period.
501   However, from 2019 to 2060, the SSP5-8.5 tends to project higher O_3 levels than SSP2-4.5. From
502   a wetting trend perspective, we must determine which pathway would project a more realistic
503   future humidity trend in NW. China has been making significant strides in transitioning to
504   renewable energy sources, reducing its carbon footprint, and committing to achieve a carbon peak
505   before 2030 and carbon neutrality by 2060. These commitments align more closely with the
506   mitigation efforts outlined in SSP2-4.5, which, as manual interventions, will overshadow the
507   impact of climate change on O_3 fluctuations. There have also been debates regarding ongoing
508   wetting trends in NW based on CMIP6 projections under SSP5-8.5 and historical data analysis
509   (Huang et al., 2017). Historically, China's rapid economic growth has heavily depended on fossil
510   fuels, which may render SSP5-8.5 more applicable in China. The responses of O_3 evolution to RH
511   under SSP5-8.5 are more akin to those observed from 1998 to 2017 (section 3.2) than to SSP2-4.5.
512   In light of this, while China may achieve its carbon peak and neutrality goals, the wetting trend in
513   NW will likely persist in the coming decades, exacerbating continuous O_3 pollution in NW, in
514   addition to manual interventions. Under SSP5-8.5, the projected increase in humidity (e.g., 34.9%
515   in Xinjiang by 2030) may enhance O_3 wet deposition, partially offsetting the warming-driven O_3
516   rise. This aligns with Li et al. (2014), who identified humidity as a critical factor modulating cross-
517   regional ozone transport efficiency.
518

519   **4. Conclusions**

520   This study conducted extensive sensitivity model simulations to explore the surface O_3
521   responses to past and future climate change in Northwestern China. The results demonstrated that
522   significant wetting since the 21st century in this region, particularly in the three westernmost
523   provinces (Xinjiang, Qinghai, and Gansu) of NW, has slowed O_3 growth. We show that in these
524   provinces, the wetting influence on O_3 evolution has outweighed the warming effect and played
525   an almost equal role to warming across the entire NW. Both factors contributed approximately 50%
526   to summer O_3 variations from 1998 to 2017, among the major meteorological factors causing
527   changes in O_3 concentrations. This finding contrasts with the dominant role of warming in the

meteorological effects on O_3 evolution in China. We linked the increasing OH radicals, which interact with water vapor, to the declining O_3 trend. Given that humidification in NW is projected to continue in the coming years and that the mitigation of O_3 precursor emissions in China will still be implemented under the nation's air pollution control strategies, the impact of humidification on O_3 trends in NW will likely become more significant. Such an impact should be considered in future policymaking for the reduction of O_3 pollution in NW. While this study advances our understanding of ozone-climate interactions in Northwestern China, several uncertainties warrant attentions. First, the reliance on static emission inventories (e.g., EDGAR) may underestimate dynamic sources such as soil NO_x emissions, which are critical in arid region. Second, the 20 km resolution of WRF-Chem may inadequately resolve fine-scale topographic effects on local meteorology (e.g., valley breezes in mountainous Northwestern China), potentially biasing ozone simulations. Future work should integrate high-resolution emission inventories to improve accuracy. Additionally, ground-based ozone measurements in remote Northwestern China remain sparse, limiting robust model validation. Expanding monitoring networks will be essential to constrain uncertainties.

Data availability

ERA-Interim reanalysis data can be accessed at https://www.ecmwf.int/en/forecasts/datasets/reanalysisdatasets/era-interim. EDGAR dataset is available at https://edgar.jrc.ec.europa.eu/. LUC data can be accessed at http://www.resdc.cn. DPEC Inventory is available at http://meicmodel.org.cn. The meteorological data under the CMIP6 framework is collected from https://aims2.llnl.gov/search/cmip6/.

Author contributions

XZ and YY contribute equally to this article. All authors contributed to the manuscript and have given approval of the final version. XZ and HG coordinated and supervised the project. XZ, YY, WW and JM designed the present experiment, carried out modeling, and drafted the manuscript. NZ, HS, XJ, CW, and HM collected the data. XZ, YY, ZY and TH analyzed simulation results.

Competing interests

The authors declare that they have no known competing financial interests or personal relationships that could have appeared to influence the work reported in this paper.

Acknowledgements

We wish to thank the High-performance Computing Platform of Peking University to support extensive model simulations of this study.

Financial support

This research was supported by the National Natural Science Foundation of China via grants 42407134, 42177351 and 41977357.

References

Bei, N. F., Zhao, L. N., Wu, J. R., Li, X., Feng, T., and Li, G. H.: Impacts of sea-land and mountain-valley circulations on the air pollution in Beijing-Tianjin-Hebei (BTH): A case study, Environ. Pollut., 234, 429–438, https://doi.org/10.1016/j.envpol.2017.11.066, 2018.

Belan, B. D., and Savkin, D. E.: The Role of Air Humidity in Variations in Near-Surface Ozone Concentration, Atmospheric and Oceanic Optics, 32, 586–589, https://doi.org/10.1134/S1024856019050038, 2019.

Bossioli, E., Tombrou, M., Kalogiros, J., Allan, J., Bacak, A., Bezantakos, S., Biskos, G., Coe, H., Jones, B. T., Kouvarakis, G., Mihalopoulos, N., and Percival, C. J.: Atmospheric composition in the Eastern Mediterranean: Influence of biomass burning during summertime using the WRF-Chem model, Atmos Environ., 132, 317–331, https://doi.org/10.1016/j.atmosenv.2016.03.011, 2016.

Cheng, J., Tong, D., Zhang, Q., Liu, Y., Lei, Y., Yan, G., Yan, L., Yu, S., Cui, R. Y., Clarke, L., Geng, G. N., Zheng, B., Zhang, X. Y., Davis, S. J., and He, K. B.: Pathways of China's $PM_{2.5}$ air quality 2015-2060 in the context of carbon neutrality, Natl. Sci. Rev., 8, nwab078, https://doi.org/10.1093/nsr/nwab078, 2021.

Cheng, J., Tong, D., Liu, Y., Geng, G. N., Davis, S. J., He, K. B., and Zhang, Q.: A synergistic approach to air pollution control and carbon neutrality in China can avoid millions of premature deaths annually by 2060, One Earth, 6, 978–989, https://doi.org/10.1016/j.oneear.2023.07.007, 2023.

Crippa, M., Guizzardi, D., Muntean, M., Schaaf, E., Dentener, F., van Aardenne, J. A., Monni, S., Doering, U., Olivier, J. G. J., Pagliari, V., and Janssens-Maenhout, G.: Gridded emissions of air pollutants for the period 1970-2012 within EDGAR v4.3.2, Earth Syst. Sci. Data, 10, 1987–2013, https://doi.org/10.5194/essd-10-1987-2018, 2018.

Cooper, O., Parrish, D., Ziemke, J., Balashov, N., Cupeiro, M., Galbally, I., Gilge, S., Horowitz, L., Jensen, N., Lamarque, J., Naik, V., Oltmans, S., Schwab, J., Shindell, D., Thompson, A., Thouret, V., Wang, Y., and Zbinden, R.: Global distribution and trends of tropospheric ozone: An observation-based review, Elementa: Science of the Anthropocene, 2, 000029, https://doi.org/10.12952/journal.elementa.000029, 2014.

Ding, J., Dai, Q., Zhang, Y., Xu, J., Huangfu, Y., and Feng, Y.: Air humidity affects secondary aerosol formation in different pathways, Sci. Total Environ., 759, 143540, https://doi.org/10.1016/j.scitotenv.2020.143540, 2021.

Ding, J., Dai, Q., Fan, W., Lu, M., Zhang, Y., Han, S., and Feng, Y.: Impacts of meteorology and precursor emission change on O_3 variation in Tianjin, China from 2015 to 2021, J. Environ. Sci., 126, 506–516, https://doi.org/10.1016/j.jes.2022.03.010, 2023.

Ding, S., Jiang, X., and Wu, C.: Contrasting near-surface ozone pollution in wet and dry year over China, Int. J. Environ. Res. Public Health, 20, 998, https://doi.org/10.3390/ijerph20020998, 2023.

Eck, T. F., Holben, B. N., Kim, J., Beyersdorf, A. J., Choi, M., Lee, S., Koo, J. H., Giles, D. M., Schafer, J. S., Sinyuk, A., Peterson, D. A., Reid, J. S., Arola, A., Slutsker, I., Smirnov, A., Sorokin, M., Kraft, J., Crawford, J. H., Anderson, B. E., Thornhill, K. L., Diskin, G., Kim, S. W., and Park, S.: Influence of cloud, fog, and

high relative humidity during pollution transport events in South Korea: Aerosol properties and $PM_{2.5}$ variability, Atmos. Environ., 232, 117530, https://doi.org/10.1016/j.atmosenv.2020.117530, 2020.

Emmons, L. K., Walters, S., Hess, P. G., Lamarque, J. F., Pfister, G. G., Fillmore, D., Granier, C., Guenther, A., Kinnison, D., Laepple, T., Orlando, J., Tie, X., Tyndall, G., Wiedinmyer, C., Baughcum, S. L., Kloster, S.: Description and evaluation of the model for ozone and related chemical tracers, version 4 (MOZART-4), Geosci. Model. Dev., 3, 43–67, https://doi.org/10.5194/gmd-3-43-2010, 2010.

Eyring, V., Bony, S., Meehl, G. A., Senior, C. A., Stevens, B., Stouffer, R. J., and Taylor, K. E.: Overview of the Coupled Model Intercomparison Project Phase 6 (CMIP6) experimental design and organization, Geosci. Model Dev., 9, 1937–1958, https://doi.org/10.5194/gmd-9-1937-2016, 2016.

Ghazali, S., Awang, N. R., Karim, M. F. A., and Muhammad, M.: Fluctuational Analysis of Nighttime Ground-Level Ozone Concentrations due to Variations in Hourly Relative Humidity, Smart Environmental Science, Technology and Management, 1, 118–121, https://doi.org/10.36647/978-93-92106-02-6.21, 2022.

Gong, C., Yue, X., Liao, H., and Ma, Y. M.: A humidity-based exposure index representing ozone damage effects on vegetation, Environ. Res. Lett., 16, 044030, https://doi.org/10.1088/1748-9326/abecbb, 2021.

Guenther, A., Karl, T., Harley, P., Wiedinmyer, C., Palmer, P. I., and Geron, C.: Estimates of global terrestrial isoprene emissions using MEGAN (Model of Emissions of Gases and Aerosols from Nature), Atmos. Chem. Phys., 6, 3181–3210, https://doi.org/10.5194/acp-6-3181-2006, 2006.

Guenther, A. B., Jiang, X., Heald, C. L., Sakulyanontvittaya, T., Duhl, T., Emmons, L. K., and Wang, X.: The Model of Emissions of Gases and Aerosols from Nature version 2.1 (MEGAN2.1): an extended and updated framework for modeling biogenic emissions, Geosci. Model Dev., 5, 1471–1492, https://doi.org/10.5194/gmd-5-1471-2012, 2012.

Han, S., Bian, H., Feng, Y., Liu, A., Li, X., Zeng, F., and Zhang, X.: Analysis of the Relationship between O_3, NO and NO_2 in Tianjin, China, Aerosol Air Qual. Res., 11, 128–139, https://doi.org/10.4209/aaqr.2010.07.0055, 2011.

Huang, J. P., Yu, H. P., Dai, A. G., Wei, Y., and Kang, L. T.: Drylands face potential threat under 2 °C global warming target, Nat. Clim. Chang., 7, 417–422, https://doi.org/10.1038/nclimate3275, 2017.

Hu, F., Xie, P., Xu, J., Lv, Y., Zhang, Z., Zheng, J., and Tian, X.: Long-term trends of ozone in the Yangtze River Delta, China: Spatiotemporal impacts of meteorological factors, local, and non-local emissions, J. Environ. Sci., 7,10–33, https://doi.org/10.1016/j.jes.2024.07.017, 2024.

Kendall, M. G.: Rank Correlation Methods, Mathematics, https://doi.org/10.2307/1402637, 1949.

Kerr, G. H., Waugh, D. W., Steenrod, S. D., Strode, S. A., and Strahan, S. E.: Surface Ozone-Meteorology Relationships: Spatial Variations and the Role of the Jet Stream, J. Geophys. Res-Atmos., 125, e2020JD032735, https://doi.org/10.1029/2020JD032735, 2020.

El-Shaarawi, A. H., and Niculescu, S. P.: On kendall's tau as a test of trend in time series data, Environmetrics, 3, 385–411, https://doi.org/10.1002/env.3170030403, 1992.

Koster, R. D., Dirmeyer, P. A., Guo, Z. C., Bonan, G., Chan, E., Cox, P., Gordon, C. T., Kanae, S., Kowalczyk, E., Lawrence, D., Liu, P., Lu, C. H., Malyshev, S., McAvaney, B., Mitchell, K., Mocko, D., Oki, T., Oleson, K., Pitman, A., Sud, Y. C., Taylor, C. M., Verseghy, D., Vasic, R., Xue, Y. K., Yamada, T., and Team, G.: Regions of strong coupling between soil moisture and precipitation, Science, 305, 1138–1140, https://doi.org/10.1126/science.1100217, 2004.

Kleeman, M. J.: A preliminary assessment of the sensitivity of air quality in California to global change, Climatic Change, 87, 273–292, https://doi.org/10.1007/s10584-007-9351-3, 2008.

Li, B., Chen, Y., and Shi, X.: Why does the temperature rise faster in the arid region of northwest China? J. Geophys. Res-Atmos., 117, D16115, https://doi.org/10.1029/2012JD017953, 2012.

Li, J., Yang, W., Wang, Z., Chen, H., Hu, B., Li, J., Sun, Y., Fu, P., Zhang, Y.: Modeling study of surface ozone source receptor relationships in East Asia, Atmos. Res. 167, 77–88, https://doi.org/10.1016/j.atmosres.2015.07.010, 2016.

Li, J. X., Wang, Z. X., Chen, L. L., Lian, L. L., Li, Y., Zhao, L. Y., Zhou, S., Mao, X. X., Huang, T., Gao, H., and Ma, J. M.: WRF-Chem simulations of ozone pollution and control strategy in petrochemical industrialized and heavily polluted Lanzhou City, NW, Sci. Total Environ., 737, 139835, https://doi.org/10.1016/j.scitotenv.2020.139835, 2020.

Li, K., Jacob, D. J., Liao, H., Shen, L., Zhang, Q., and Bates, K. H.: Anthropogenic drivers of 2013-2017 trends in summer surface ozone in China, Proc. Natl. Acad. Sci. U.S.A., 116, 422–427, https://doi.org/10.1073/pnas.1812168116, 2019.

Li, K., Jacob, D. J., Liao, H., Qiu, Y. L., Shen, L., Zhai, S. X., Bates, K. H., Sulprizio, M. P., Song, S. J., Lu, X., Zhang, Q., Zheng, B., Zhang, Y. L., Zhang, J. Q., Lee, H. C., and Kuk, S. K.: Ozone pollution in the North China Plain spreading into the late-winter haze season, Proc. Natl. Acad. Sci. U.S.A., 118, e2015797118, https://doi.org/10.1073/pnas.2015797118, 2021.

Li, K., Jacob, D. J., Shen, L., Lu, X., De Smedt, I., and Liao, H.: Increases in surface ozone pollution in China from 2013 to 2019: anthropogenic and meteorological influences, Atmos. Chem. Phys., 20, 11423–11433, https://doi.org/10.5194/acp-20-11423-2020, 2020.

Li, L., Liu, N., Shen, L., Zhao, Z., Wang, H., Wang, Y., Li, X., and Ma, Y.: Ozone concentration at various heights near the surface layer in Shenyang, Northeast China, Front. Environ. Sci., 10, 1011508, https://doi.org/10.3389/fenvs.2022.1011508, 2022.

Li, M., Yu, S., Chen, X., Li, Z., Zhang, Y., Wang, L., Liu, W., Li, P., Lichtfouse, E., Rosenfeld, D., and Seinfeld, J. H.: Large scale control of surface ozone by relative humidity observed during warm seasons in China, Environ. Chem. Lett., 19, 3981–3989, https://doi.org/10.1007/s10311-021-01265-0, 2021.

Li, X., Liu, J., Mauzerall, D. L., Emmons, L. K., Walters, S., Horowitz, L. W., Tao, S.: Effects of trans-Eurasian transport of air pollutants on surface ozone concentrations over Western China, J. Geophys. Res. Atmos., 119, 12338–12354, https://doi.org/10.1002/2014JD021936, 2014.

Li, X. B., Yuan, B., Parrish, D. D., Chen, D. H., Song, Y. X., Yang, S. X., Liu, Z. J., and Shao, M.: Long-term trend of ozone in southern China reveals future mitigation strategy for air pollution, Atmos. Environ., 269, 118869, https://doi.org/10.1016/j.atmosenv.2021.118869, 2022.

Lian, X., Piao, S. L., Chen, A. P., Huntingford, C., Fu, B. J., Li, L., Huang, J. P., Sheffield, J., Berg, A. M., Keenan, T. F., McVicar, T. R., Wada, Y., Wang, X. H., Wang, T., Yang, Y. T., and Roderick, M. L.: Multifaceted characteristics of dryland aridity changes in a warming world, Nat. Rev. Earth Env., 2, 232–250, https://doi.org/10.1038/s43017-021-00144-0, 2021.

Liao, J. B., Wang, T. J., Jiang, Z. Q., Zhuang, B. L., Xie, M., Yin, C. Q., Wang, X. M., Zhu, J. L., Fu, Y., and Zhang, Y.: WRF/Chem modeling of the impacts of urban expansion on regional climate and air pollutants in Yangtze River Delta, China, Atmos. Environ., 106, 204–214, https://doi.org/10.1016/j.atmosenv.2015.01.059, 2015.

Liu, X., Zhang, D., Luo, Y., and Liu, C.: Spatial and temporal changes in aridity index in northwest China: 1960 to 2010, Theor. Appl. Climatol., 112, 307–316, https://doi.org/10.1007/s00704-012-0734-7, 2013.

Lu, X., Ye, X. P., Zhou, M., Zhao, Y. H., Weng, H. J., Kong, H., Li, K., Gao, M., Zheng, B., Lin, J. T., Zhou, F., Zhang, Q., Wu, D. M., Zhang, L., and Zhang, Y. H.: The underappreciated role of agricultural soil nitrogen oxide emissions in ozone pollution regulation in North China, Nat. Commun., 12, 5021, https://doi.org/10.1038/s41467-021-25147-9, 2021.

Ma, S., Shao, M., Zhang, Y., Dai, Q., and Xie, M.: Sensitivity of $PM_{2.5}$ and O_3 pollution episodes to meteorological factors over the North China Plain, Sci. Total. Environ., 792, 148474, https://doi.org/10.1016/j.scitotenv.2021.148474, 2021.

Madden, R. A., and Williams, J.: The Correlation between Temperature and Precipitation in the United States and Europe, Mon. Weather Rev., 106, 142–147, https://doi.org/10.1175/1520-0493(1978)106<0142:TCBTAP>2.0.CO;2, 1978.

Mann, H. B.: Nonparametric Tests Against Trend, Econometrica, 13, 245, https://doi.org/10.2307/1907187, 1945.

Millstein, D. E., and Harley, R. A.: Impact of climate change on photochemical air pollution in Southern California, Atmos. Chem. Phys., 9, 3745–3754, https://doi.org/10.5194/acp-9-3745-2009, 2009.

Mo, J. Y., Huang, T., Zhang, X. D., Zhao, Y., Liu, X., Li, J. X., Gao, H., and Ma, J. M.: Spatiotemporal distribution of nitrogen dioxide within and around a large-scale wind farm - a numerical case study, Atmos. Chem. Phys., 17, 14239–14252, https://doi.org/10.5194/acp-17-14239-2017, 2017.

Nie, J. S., Wang, W. H., Heermance, R., Gao, P., Xing, L., Zhang, X. J., Zhang, R., Garzione, C., and Xiao, W. J.: Late Miocene Tarim desert wetting linked with eccentricity minimum and East Asian monsoon weakening, Nat. Commun., 13, 3977, https://doi.org/10.1038/s41467-022-31577-w, 2022.

Peng, D., and Zhou, T.: Why was the arid and semiarid northwest China getting wetter in the recent decades? J. Geophys. Res-Atmos., 122, 9060–9075, https://doi.org/10.1002/2016JD026424, 2017.

Pfannerstill, E. Y., Arata, C., Zhu, Q., Schulze, B. C., Ward, R., Woods, R., Harkins, C., Schwantes, R. H., Seinfeld, J. H., Bucholtz, A., Cohen, R. C., and Goldstein, A. H.: Temperature-dependent emissions dominate aerosol and ozone formation in Los Angeles, Science, 384, 1324–1329, https://doi.org/10.1126/science.adg8204, 2024.

Shi, P. Y., Tilgner, M., and Lo, M. K.: Construction and characterization of subgenomic replicons of New York strain of West Nile virus, Virology, 296, 219–233, https://doi.org/10.1006/viro.2002.1453, 2002.

Tie, X., Madronich, S., Li, G., Ying, Z., Weinheimer, A., Apel, E., and Campos, T.: Simulation of Mexico City plumes during the MIRAGE-Mex field campaign using the WRF-Chem model, Atmos Chem. Phys., 9, 4621–4638, https://doi.org/10.5194/acp-9-4621-2009, 2009.

Tong, D., Cheng, J., Liu, Y., Yu, S., Yan, L., Hong, C. P., Qin, Y., Zhao, H. Y., Zheng, Y. X., Geng, G. N., Li, M., Liu, F., Zhang, Y. X., Zheng, B., Clarke, L., and Zhang, Q.: Dynamic projection of anthropogenic emissions in China: methodology and 2015-2050 emission pathways under a range of socio-economic, climate policy, and pollution control scenarios, Atmos. Chem. Phys., 20 (9), 5729–5757, https://doi.org/10.5194/acp-20-5729-2020, 2020.

Wang, J., Li, J., Li, X., Wang, D., and Fang, C.: Relationship between ozone and air temperature in future conditions: A case study in Sichuan basin, China, Environ. Pollut., 343, 123276, https://doi.org/10.1016/j.envpol.2023.123276, 2024.

Wang, Z. B., Li, J. X., and Liang, L. W.: Spatio-temporal evolution of ozone pollution and its influencing factors in the Beijing-Tianjin-Hebei Urban Agglomeration, Environ. Pollut., 256, 113419, https://doi.org/10.1016/j.envpol.2019.113419, 2020.

Wild, O., Zhu, X., and Prather, M. J.: Fast-J: Accurate Simulation of In- and Below-Cloud Photolysis in Surface Chemical Models, J. Atmos. Chem., 37, 245–282, https://doi.org/10.1023/A:1006415919030, 2000.

Yan, D., Jin, Z. P., Zhou, Y. T., Li, M. M., Zhang, Z. H., Wang, T. J., Zhuang, B. L., Li, S., and Xie, M.: Anthropogenically and meteorologically modulated summertime ozone trends and their health implications since China's clean air actions, Environ. Pollut., 343, 123234, https://doi.org/10.1016/j.envpol.2023.123234, 2024.

Yang, P., Xia, J., Zhang, Y. Y., and Hong, S.: Temporal and spatial variations of precipitation in Northwest China during 1960-2013, Atmos. Res., 183, 283–295, https://doi.org/10.1016/j.atmosres.2016.09.014, 2017.

Yang, X. Y., Li, D. W., Yang, Z., Wu, K., Ji, L. Y., Zhou, Z. Q., and Lu, Y. Q.: Revealing historical observations and future projections of precipitation over Northwest China based on dynamic downscaled CMIP6 simulations, Front. Earth Sci., 10, 1090221, https://doi.org/10.3389/feart.2022.1090221, 2023.

741 Yao, J. Q., Mao, W. Y., Chen, J., and Dilinuer, T.: Recent signal and impact of wet-to-dry climatic shift in
742 Xinjiang, China, J. Geog. Sci., 31, 1283–1298, https://doi.org/10.1007/s11442-021-1898-9, 2021.

743 Yu, R. X., Liu, M. X., Li, L., Song, J. Y., Sun, R. D., Zhang, G. J., Xu, L., and Mu R. L.: Spatial and Temporal
744 Variation of Atmospheric Ozone Column Concentration and Influencing Factors in the Yangtze River Delta
745 Region in Recent 15 Years, Acta Scientiae Circumstantiae, 41, 770–784,
746 https://doi.org/10.13671/j.hjkxxb.2020.0346, 2021.

747 Zhang, X. D., Du, J., Zhang, L. M., Huang, T., Gao, H., Mao, X. X., and Ma, J. M.: Impact of afforestation on
748 surface ozone in the North China Plain during the three-decade period, Agric. For. Meteorol., 287,
749 https://doi.org/10.1016/j.agrformet.2020.107979, 107979, 2020.

750 Zhang, X. D., Jian, X. H., Zhao, Y., Liu, X. R., Chen, K. J., Wang, L. F., Tao, S., Liu, J. F., Huang, T., Gao, H.,
751 Liu, Y. J., Zhugu, R. R., and Ma, J. M.: Tropospheric Ozone Perturbations Induced by Urban Land
752 Expansion in China from 1980 to 2017, Environ. Sci. Technol., 56, 6978–6987,
753 https://doi.org/10.1021/acs.est.1c06664, 2022.

754 Zhang, X. D., Zhugu, R. Y., Jian, X., Liu, X., Chen, K., Tao, S., Liu, J., Gao, H., Huang, T., and Ma, J. M.:
755 Associations of interannual variation in summer surface ozone with the Western Pacific Subtropical High
756 in China from 1999 to 2017, Atmos. Chem. Phys., 23, 15629–15642, https://doi.org/10.5194/acp-23-15629-
757 2023, 2023.